Received 3 July 2025; accepted 22 July 2025. Date of publication 30 July 2025; date of current version 24 November 2025.
Digital Object Identifier 10.1109/OJAP.2025.3593894

Analysis of LEO Satellite Detection Errors Considering Atmospheric Environment

JONGHO KEUN [1], DOYOUNG JANG [2], AND HOSUNG CHOO [1] (Senior Member, IEEE)

[1] Department of Electronic and Electrical Engineering, Hongik University, Seoul 04066, Republic of Korea
[2] Department of Information and Communication Engineering, Dongyang Mirae University, Seoul 08221, Republic of Korea

CORRESPONDING AUTHOR: D. JANG (e-mail: dyjang2023@dongyang.ac.kr)

This work was supported by the Korea Institute for Advancement of Technology funded by the Korea Government (Ministry of Education) under Grant P0028167.

ABSTRACT This paper proposes a ray-tracing method to estimate a propagation path between a ground station and low-Earth-orbit (LEO) satellites. To accurately predict a propagation path and detection error, the proposed ray-tracing method adopts an atmospheric refractivity model that includes not only the troposphere but also the ionosphere. Herein, atmospheric refractivity in the troposphere is the measurement data obtained from weather observatories in Korea. In addition, atmospheric refractivity in the ionosphere is obtained from the simplified Appleton-Hartree equation. The detection angle errors are examined by changing various conditions, such as the locations of ground stations, satellite trajectories, and observation date. For the trajectories of the KOMPSAT-5 satellite, the maximum detection angle errors observed at inland and coastal meteorological observatories are 309 mdeg and 331 mdeg, respectively. The results demonstrate that the proposed ray-tracing method is suitable for determining the propagation path between the ground station and LEO satellites.

INDEX TERMS Space surveillance, atmospheric propagation, LEO satellite, ray-tracing, atmospheric refraction model.

I. INTRODUCTION

LOW-EARTH-ORBIT (LEO) satellite technologies have become increasingly useful for various applications, such as satellite broadcasting, Earth observation, and mobile communications [1], [2]. A large number of satellites, approximately 8,000, operate at altitudes from 160 to 2,000 km, which may increase the risk of collisions between operational satellites [3], [4], [5]. Therefore, many organizations, such as the National Aeronautics and Space Administration (NASA) and the European Space Agency (ESA), continuously track satellites to predict potential collisions in advance. To track the location of LEO satellites, ground stations utilize space surveillance radars with high-gain characteristics, such as reflector antennas or phased array antennas [6], [7], [8], [9]. In Earth's atmosphere, the propagation paths of the electromagnetic waves emitted by radars may be refracted, which can significantly reduce the tracking performance of space surveillance radars. Therefore, a method that can estimate a propagation path while considering atmospheric refraction is required to reduce tracking error.

The parabolic equation (PE) method can effectively estimate a radar's propagation path because it can consider the atmospheric refractive index and ground effects. Therefore, studies using the PE method to estimate various radar propagation scenarios, such as ground-to-ground, ground-to-air, and air-to-air, have been reported [10], [11], [12]. However, the PE method can only provide reliable results when a radar's steering elevation angle is within 15° [13], [14].

In contrast, the ray-tracing method can effectively analyze a wave propagation path for all the steering elevation angles of a radar. Therefore, the ray-tracing method is suitable for estimating the propagation path between a ground station and LEO satellites. PHaRLAP simulation software based on the ray-tracing method is utilized to analyze this propagation path [15], [16].

Although these studies focused on changes in the wave propagation path caused by the refractive index of the ionosphere, they did not consider the tropospheric environment, which can also affect wave propagation. Conversely, some studies have considered only the troposphere, neglecting ionospheric effects [17], [18]. To analyze the effect on the entire region between a ground station and LEO satellites, the Niell function and the Klobuchar model have been used in some previous studies, which can estimate signal delays between a ground station and LEO satellites by considering both the troposphere and ionosphere [19], [20], [21]. However, there is a lack of research analyzing the propagation paths of radar waves based on an actual satellite trajectory.

In this paper, we propose a ray-tracing method to estimate the propagation path between a ground station and LEO satellites. The proposed ray-tracing method uses an atmospheric refractivity model that includes not only the troposphere but also the ionosphere. This refractive index model enables accurate estimation of the ray-path across the entire 0–600 km altitude range. Herein, atmospheric refractivity in the troposphere is the measurements data obtained from weather observatories in Korea. In addition, atmospheric refractivity in the ionosphere is obtained from the simplified Appleton-Hartree equation [22], and this equation utilizes the electron density data of the NeQuick2 model [23].

Then, we conduct a tracking simulation using real satellite trajectories to predict detection errors in real satellite tracking scenarios. The trajectories of the LEO satellites use the consolidated prediction format (CPF) data of the KOMPSAT-5 satellite provided by NASA. In these trajectories, the position of an LEO satellite is converted to an east-north-up (ENU) coordinate system based on a ground station. Then, the detection angle errors over the tracking time for a satellite are calculated by comparing a refracted path with a non-refracted path. The detection angle errors are examined by changing various conditions, such as the locations of a ground station, satellite trajectories, and observation dates. The results demonstrate that the proposed estimation method is suitable for predicting the propagation path and detection error of a ground station's space surveillance radar.

II. ANALYSIS OF LEO SATELLITE DETECTION ANGLE ERROR USING RAY-TRACING METHOD

Fig. 1 illustrates the propagation path between the space surveillance radar of a ground station and an LEO satellite. The electromagnetic waves emitted by a space surveillance radar propagate into the atmosphere to track LEO satellites in space orbit. These electromagnetic waves may propagate with refraction due to variations in the atmospheric refractive index. The refraction of electromagnetic waves in the troposphere occurs due to changes in the refractive index of the atmosphere according to altitude (h). Then, free electrons distributed in the ionosphere also refract electromagnetic waves. On the other hand, the stratosphere has a stable atmosphere, so electromagnetic waves are barely refracted. Therefore, to accurately track the location of an LEO satellite, it is necessary to estimate the detection angle errors of space surveillance radars by applying an atmospheric refractivity model that includes the troposphere and the ionosphere.

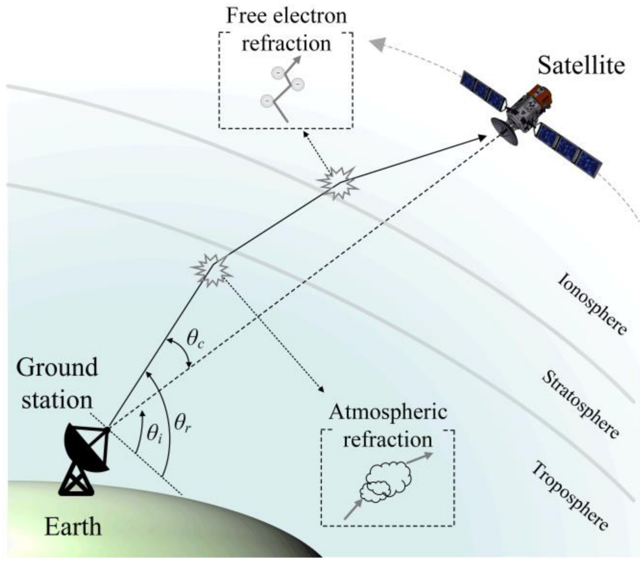

FIGURE 1. Propagation path of a radar signal in the atmosphere for an LEO satellite tracking scenario.

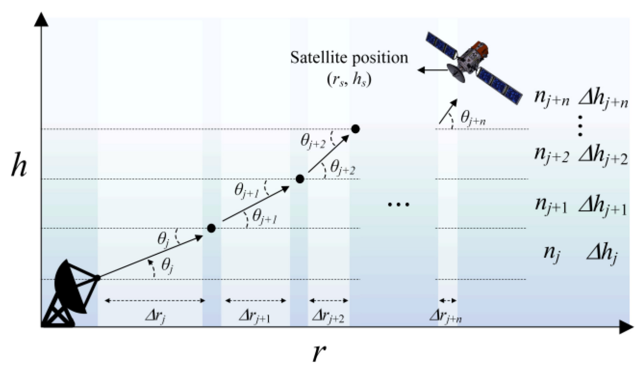

FIGURE 2. The ray-tracing method for wave path analysis considering atmospheric refractive index.

In this scenario, propagation paths can be defined as ideal paths and real paths. An ideal path is a straight line between a radar and an LEO satellite, assuming no atmospheric refraction. A real path is the refracted path caused by atmospheric refraction in the atmosphere. Herein, the steering elevation angle of the ground station for the ideal and real paths are θ_i and θ_r, respectively. The detection angle error of θ_c is determined by the difference between θ_i and θ_r, as shown in Fig. 1.

Fig. 2 explains the ray-tracing method used to analyze the real propagation path of an electromagnetic wave in the atmosphere. The ray tracing method can achieve high accuracy even at high steering angles, making it suitable for analyzing the propagation path of space surveillance radar [14]. As can be seen in Fig. 2, the entire ray path is calculated by dividing the path into several ray segments, and the path of the j-th segment is determined by Δr_j and Δh_j. In this analysis, Δh_j for all the segments is set to 1 m, and Δr_j is calculated considering the atmospheric refractive index as follows [24], [25]:

$$\theta_{j+1} = \sin^{-1}\left(\frac{n_j}{n_{j+1}}\sin\,\theta_j\right) \tag{1}$$

$$\Delta r_{j+1} = \frac{\Delta h_{j+1}}{\tan\,\theta_{j+1}} \tag{2}$$

where n_j is the atmospheric refractive index for the j-th segment, and θ_j is the angle between the r-axis and the j-th segment. Therefore, θ_j, which indicates the direction of the ray segment, is updated according to the change in the atmospheric refractive index with altitude. Then, the entire ray path can be obtained by iteratively updating the ray segments until the boundary of the analysis area.

Even if the radar is accurately steered to the target's location, the propagating waves may not reach the target due to atmospheric refraction along the propagation path. Therefore, the steering angle should be adjusted to find the ray path that reaches the target. Fig. 3 shows the process used to find the steering angle at which a ray can reach a target. To solve this, we utilize the binary search method [26], which finds a ray that reaches the target through the following procedure: First, several rays are generated with a steering angle ranging from 0° to 90° at intervals of θ_d, and two rays adjacent to the satellite are then selected, as shown in Fig. 3(a). After selecting these adjacent rays, the area between the steering angles θ_{s1} and θ_{s2} that generate each ray is designated as a binary search area. In this area, the distances l_{sn} are calculated for adjacent ray 1 (generated at θ_{s1}) and adjacent ray 2 (generated at θ_{s2}), respectively. Herein, the steering angle θ_{sn} of the ray with a greater distance l_n is updated using the following equation:

$$\theta_{sn} = \frac{\theta_{sa} + \theta_{sb}}{2} \tag{3}$$

For example, if the l_2 of a ray generated at θ_{s2} is greater than the l_1 of a ray generated at θ_{s1}, the steering angle θ_{s2} is updated as θ_{s3}, as shown in Fig. 3(b). Then, l_1 and l_3 are compared between the rays generated at angles θ_{s1} and θ_{s3} again. If the l_3 for θ_{s3} is greater than l_1 for θ_{s1}, the steering angle θ_{s3} is recalculated to θ_{s4}. By repeating this process, the ray progressively gets closer to the target, as shown in Fig. 3(b). If the distance l_n between the ray and a satellite's position is less than 1 m, the ray is assumed to have reached the satellite.

Fig. 4 presents the atmospheric refractivity model with respect to the altitude (h) for use in the proposed ray tracing method. This model includes refractive indices for all layers of the atmosphere, including the troposphere ($h <$ 30 km), stratosphere (30 km $< h <$ 80 km), and ionosphere ($h >$ 80 km), as follows [27], [28]:

$$n = \begin{cases} (77.6\times10^{-6}\times\frac{P}{T} + 0.373\times\frac{e}{T^2}) + 1, & h < 30\ km \\ 1, & 30\ km \leq h < 80\ km \\ \sqrt{1 - \frac{1}{\omega_0^2}\frac{{N_e}^2}{\varepsilon_0 m_e}}, & 80\ km \leq h \leq 600\ km \end{cases} \tag{4}$$

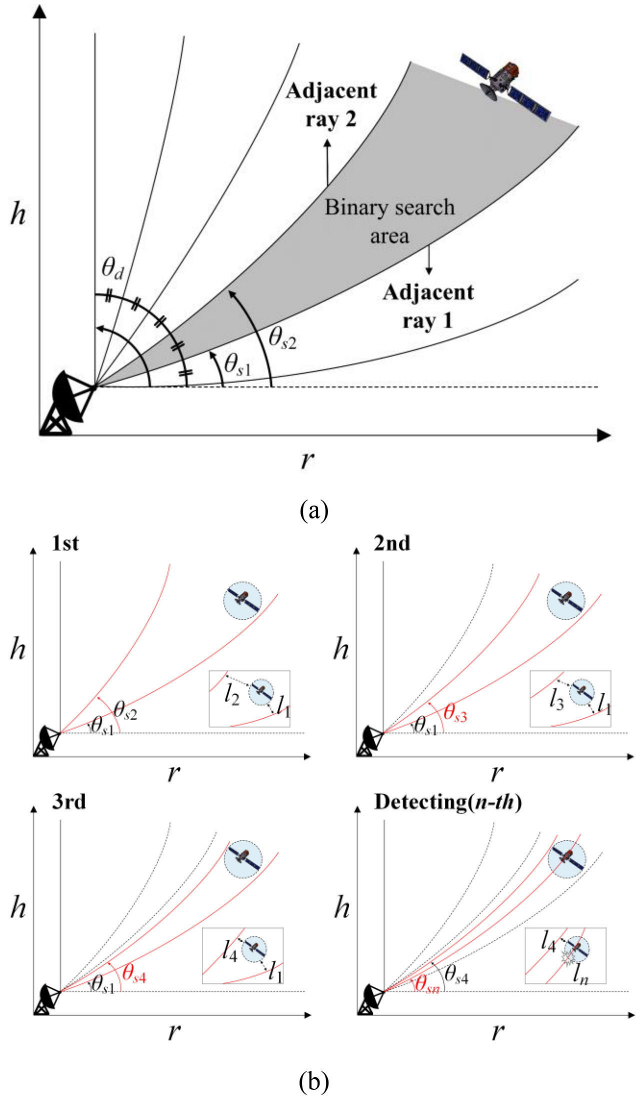

FIGURE 3. Binary search method in the ray-tracing method. (a) adjacent two-rays selection. (b) finding a path that reaches a target.

In the troposphere, atmospheric density decreases with increasing altitude, allowing the tropospheric refractive index to be calculated from meteorological data, including air pressure (P), absolute temperature (T), and water vapor pressure (e). Therefore, we collect meteorological data from meteorological observatories in Korea. This data enables statistical analysis of detection angle errors with respect to seasonal and regional characteristics. Then, the stratosphere is assumed to be 1 from h = 30 km to h = 80 km, which means that the stratosphere has no atmospheric refraction because it has a stable atmosphere [29]. On the other hand, the ionosphere is the region where electromagnetic waves are refracted by free electrons, even though the atmospheric density is very low. Therefore, the refractive index in the ionosphere is calculated using the simplified Appleton-Hartree equation. This equation uses the electron density (N_e), electron mass (m_e), angular velocity (ω at a frequency of 3 GHz), and absolute permittivity (ε_0) [30]. The electron

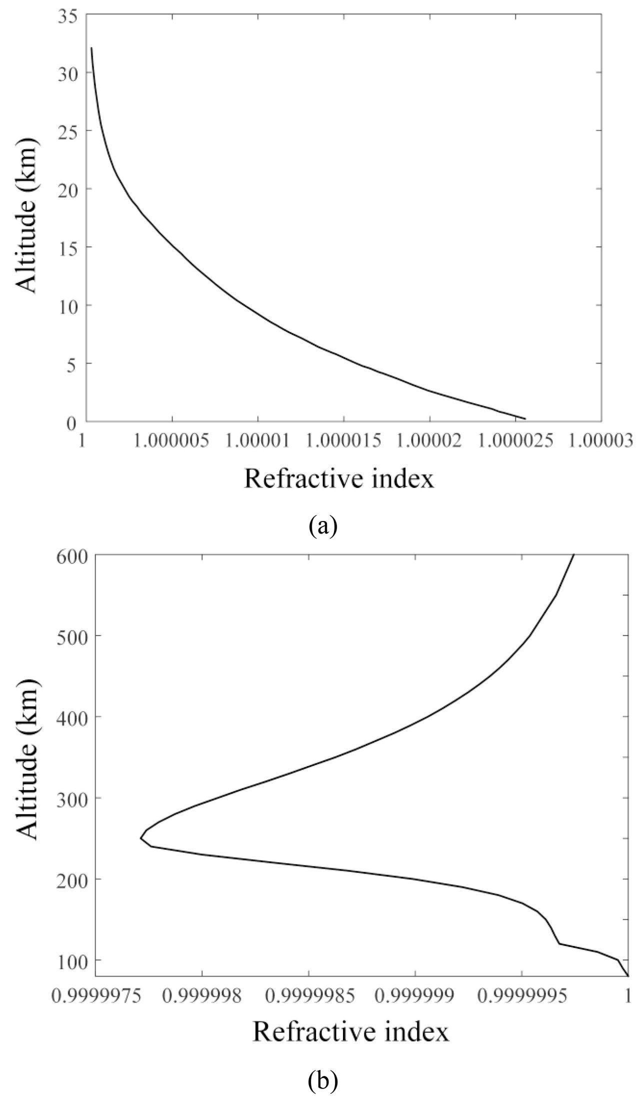

FIGURE 4. **Atmospheric refractivity from the troposphere to the ionosphere (Jan. 1, 2019). (a) in the troposphere ($h = 0$ to 32 km). (b) in the ionosphere ($h = 80$ km to 600 km).**

density data can be obtained from the NeQuick2 model provided by the ITU-R. (P.531-12). Therefore, the atmospheric refractivity model applied in the proposed ray-tracing method contains all the atmospheric refractivity information from 0 to 600 km in altitude, which helps to accurately predict the propagation path between the ground station and the LEO satellite.

Fig. 5 shows the propagation path according to the steering angle, considering the effects of atmospheric refraction. The radar's elevation steering angles are set to 0.5°, 1°, and 10°, respectively. In this analysis, atmospheric conditions are assumed to be a standard condition [31], and the results of the proposed method are compared with those of the Advanced Refractive Effects Prediction System (AREPS) simulation to verify its accuracy [32]. The ray-tracing simulations are performed using MATLAB R2023a, and average computation time for each ray path is 79 seconds (Intel Core i7-12700F CPU and 128 GB RAM). The blue solid line and the red dashed line represent the propagation paths calculated using the proposed method and the AREPS simulator, respectively. In addition, the green dotted line indicates the propagation path without refraction (ideal path).

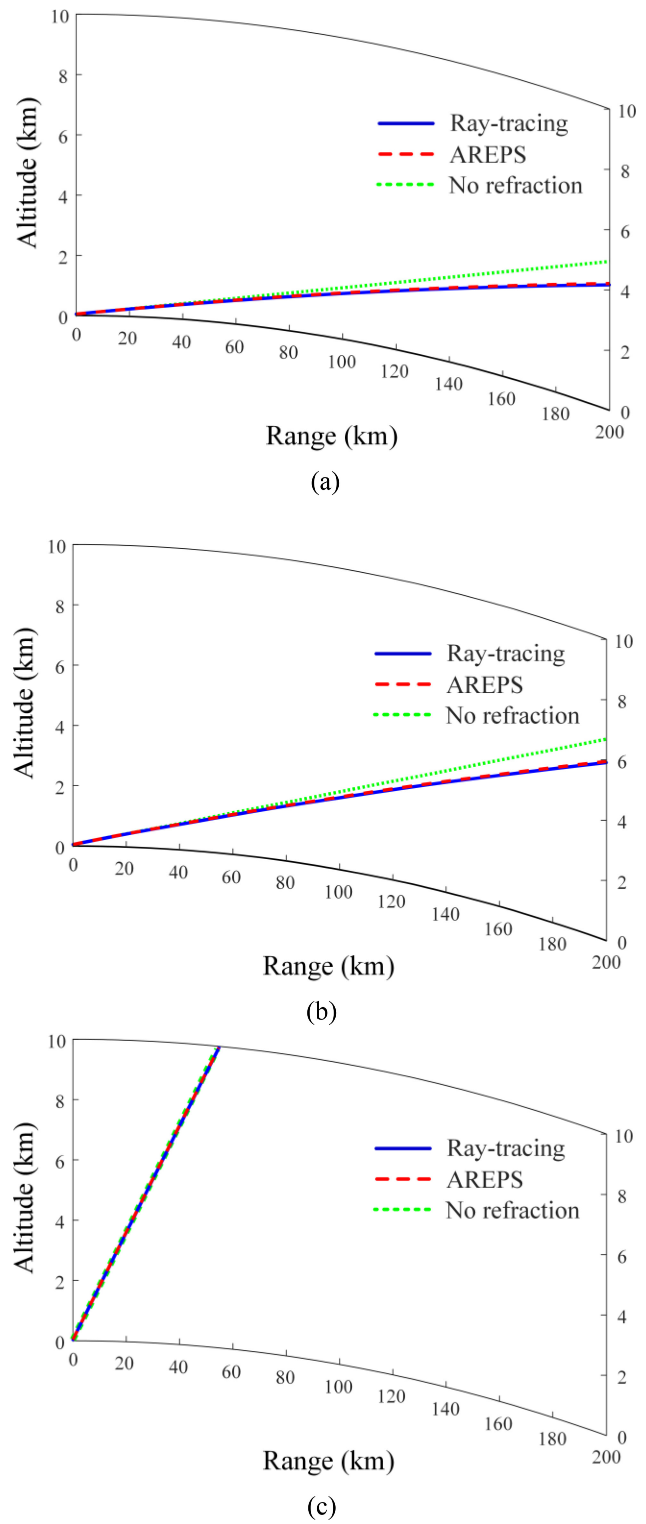

FIGURE 5. **Comparison of propagation paths based on elevation steering angle with the proposed method and AREPS simulation. (a) steering angle = 0.5°. (b) steering angle = 1°. (c) steering angle = 10°.**

TABLE 1. Detection angle error in temperate continental air.

Elevation angle	2°	10°	20°
ITU-R P.834-9	360 mdeg	110 mdeg	50 mdeg
Proposed method	355.8 mdeg	101.5 mdeg	49 mdeg

As can be seen in Fig. 5(a), when the steering angle is 0.5°, the electromagnetic wave has a slightly refracted path. Therefore, at a range of 200 km, the difference in elevation between the ideal and actual paths (using ray-tracing) is 780 m. On the other hand, if the steering angle is 1°, the altitude difference is reduced to 776 m under the same conditions, as shown in Fig. 5(b). When the steering angle is 10°, the electromagnetic waves have a nearly straight path, as shown in Fig. 5(c). In addition, when comparing the results of the proposed method with AREPS, the altitude differences for steering angles of 0.5° and 1° are 0.14 m and 0.009 m at a range of 200 km, respectively. Similarly, a small altitude difference of 0.006 m is observed at a range of 50 km in the steering angle of 10°. The result means that the propagation path using the proposed method is in good agreement with the AREPS result.

Table 1 provides the detection error results when using the ITU-R model (P.834-9) and the proposed method, respectively. In this analysis, ITU-R is temperate continental air conditions, and the proposed method is applied under inland conditions (Jan. 1, 2019, Osan) [33].

The steering angles of the radar are assumed to be of 2°, 10°, and 20°, respectively, and the expected detection errors using the ITR model for each steering angle are 360 mdeg, 110 mdeg, and 50 deg. The estimation results using the proposed method under the same conditions are 355.8 mdeg, 101.5 mdeg, 49 mdeg. Despite the difficulties in using real measurement data for validating radar detection angle errors, the analysis demonstrates that the proposed method provides highly reliable results.

III. CALCULATION DETECTION ANGLE ERROR

Fig. 6 shows the detection angle errors and a radar's steering angle according to the range between a ground station and an LEO satellite. The altitude of the satellite is fixed at 500 km, and the range increases from 800 km to 1000 km. The solid line indicates the detection angle errors (left y-axis) with respect to the range, and the dashed line is the steering angle (right y-axis) between the ground station and the LEO satellite. As the satellite's altitude increases from 800 km to 1,000 km, the radar's steering angle decreases from 32° to 26.6°. In contrast, the detection angle error increases gradually from 28.8 mdeg to 38.7 mdeg. The analysis indicates that the troposphere has a greater influence on wave refraction than the ionosphere; however, the ionospheric contribution is not negligible.

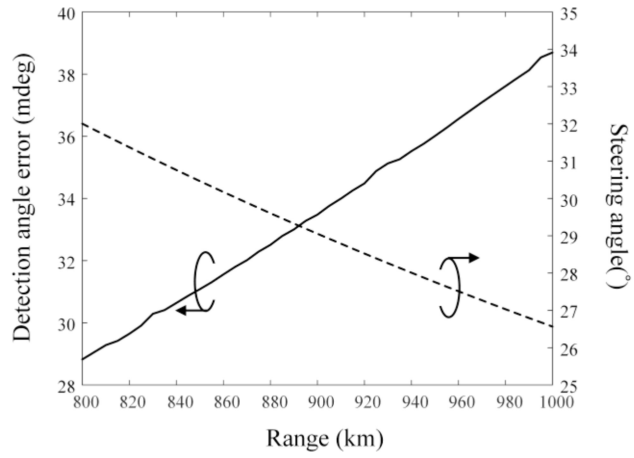

FIGURE 6. Detection angle error and a radar's steering angle according to range.

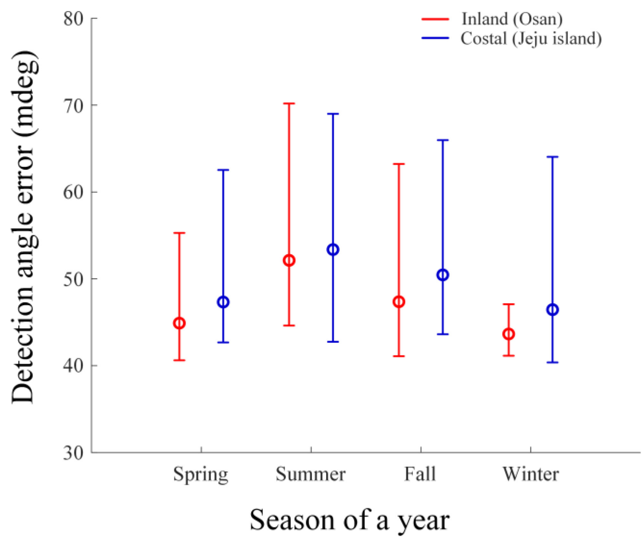

FIGURE 7. Error bar plot for detection angle error according to seasonal and regional atmosphere environments.

Fig. 7 presents the error bar plot for the detection angle error where the surveillance radar is located at the inland region (Osan) and the coastal region (Jeju Island). The circular markers indicate the average errors, and the vertical lines mean the deviation (difference between the maximum and minimum values) of angle errors. For this analysis, we use four-season meteorological data covering spring (Mar. 1, 2019 to May 30, 2019), summer (Jun. 1, 2019 to Aug. 30, 2019), fall (Sep. 1, 2019 to Nov. 30, 2019), and winter (Jan. 1, 2019 to Feb. 28, and Dec, 2019). In addition, the position of the satellite is fixed at a range of 1000 km and an altitude of 500 km. At the inland region, the average and deviation of detection error during winter are 43.7 mdeg and 5.9 mdeg, respectively. On the other hand, during summer, an average error of 51.9 mdeg and a deviation of 25.5 mdeg are observed, which are higher than the average detection error during winter. In addition, the average error in the coastal region is higher than that in the inland region across

TABLE 2. Detection angle error values according to seasonal and regional atmosphere environment.

	Spring	Summer	Fall	Winter
Inland	44.9 mdeg	52.1 mdeg	47.4 mdeg	43.7 mdeg
Costal	47.3 mdeg	53.4 mdeg	50.5 mdeg	46.5 mdeg

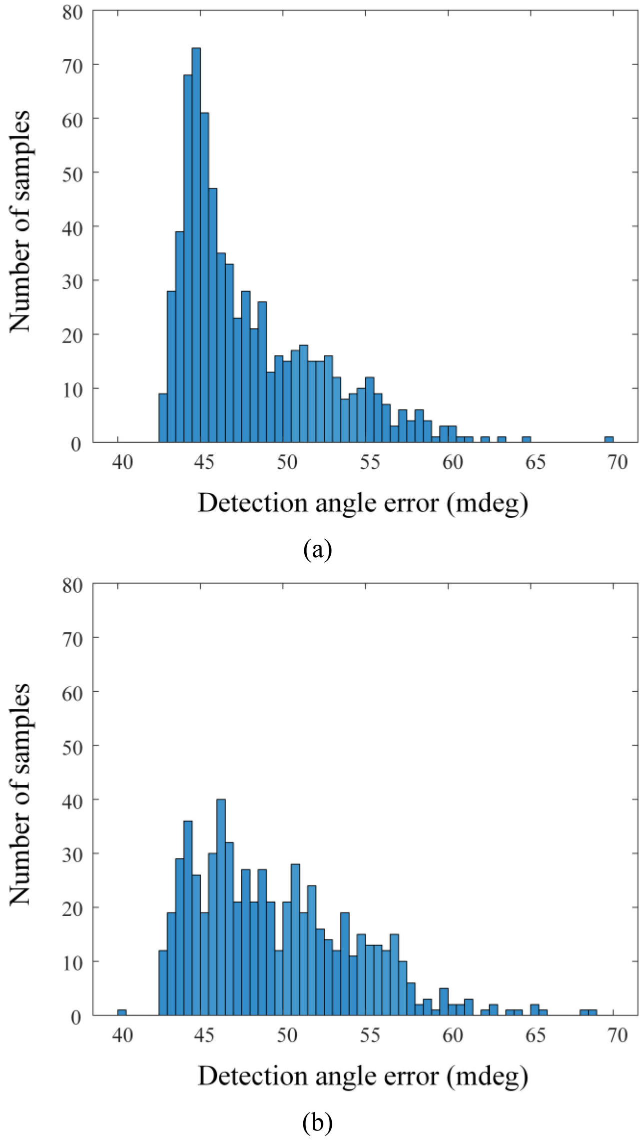

FIGURE 8. Histogram of the detection angle error according to ground station position. (a) in inland region (Osan). (b) in coastal region (Jeju Island).

all seasons. The values of the seasonal and regional detection angle errors in 2019 are listed in Table 2.

Fig. 8 represents a histogram of the detection angle errors according to the location of the ground station. In this histogram, we utilize the same data and conditions as in Fig. 7, and the bar width is set to 0.5 mdeg. In Fig. 8(a), the detection angle error between 44.5 mdeg and 45 mdeg occurs

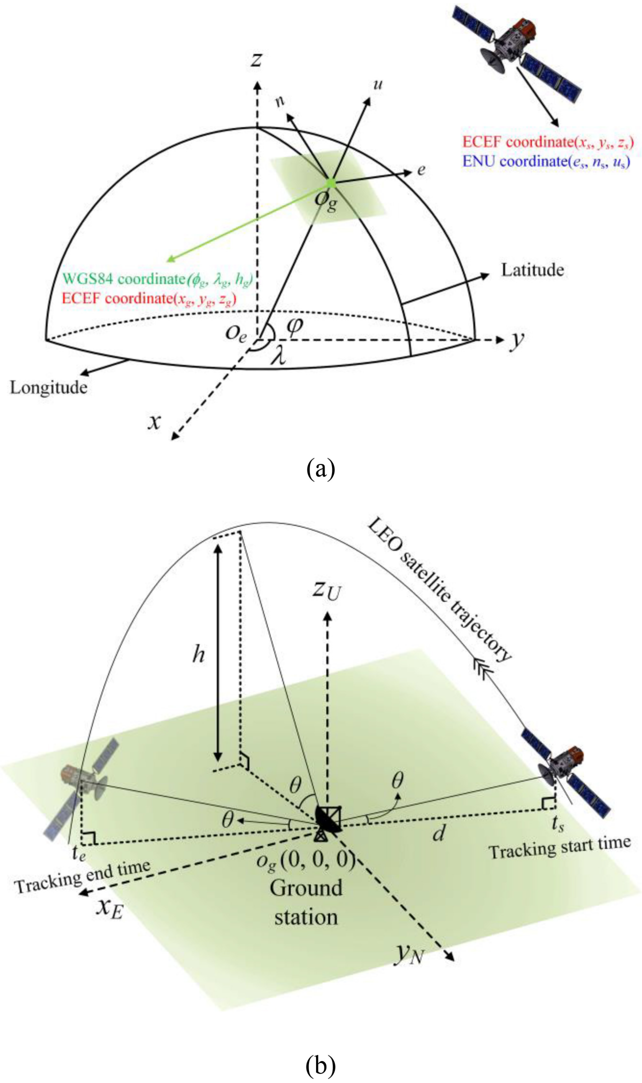

FIGURE 9. Coordinate systems for the LEO satellite tracking scenario: (a) coordinate conversion of ECEF to ENU. (b) satellite tracking scenario.

a maximum of 73 times in the inland region. In addition, the variance of the detection angle error in the inland region is calculated as 0.00005. In the coastal region, the highest error occurrence is 40 times, from 46 mdeg to 46.5 mdeg, and the variance of the error is 0.000263, as shown in Fig. 8(b). The results indicate that the detection angle errors in the coastal region are more disturbed than in the inland region. The large deviations in detection angle errors observed in coastal regions are primarily attributed to convective activity, which induces frequent variations in the refractive index. In contrast, the atmosphere over inland areas tends to be more stable, leading to smaller deviations in detection angle error.

Fig. 9 illustrates the coordinate systems for a LEO satellite tracking scenario. To simulate a situation in which an actual satellite is tracked by a ground station, information about the ground station's position and satellite trajectory is required. In addition, this information must be expressed in the ENU coordinate system with the location of the ground station as the origin (O_g). To obtain information for the satellite trajectory, we use the CPF data of KOMPSAT-5 provided by NASA. Since the CPF data includes actual satellite trajectory information, it allows us to realistically model the trajectory of the detected satellite. However, this data consists of the Earth-centered Earth-fixed (ECEF) coordinate system (x, y, z), which has the Earth's center of gravity as the origin (O_e), as shown in Fig. 9(a). Furthermore, a ground station's location is typically given in the WGS84 coordinate system, which consists of latitude, longitude, and altitude. Therefore, the ground station's coordinates must first be converted to the ECEF coordinate system using the following equations [34]:

$$N = \frac{a}{\sqrt{1 - e^2 \sin^2 \phi_g}} \tag{5}$$

$$\begin{aligned} x_g &= (N + h) \cos \phi_g \cos\lambda_g \\ y_g &= (N + h) \cos \phi_g \sin\lambda_g \\ z_g &= ((1 - e^2)N + h_g) \sin \phi_g \end{aligned} \tag{6}$$

where N is the radius of the Earth, a is the ellipsoidal equatorial radius (= 6378.137 km for WGS84), e is the eccentricity of the ellipsoid ($e^2 = 0.00669437999$ for WGS84), φ_g is the latitude, λ_g is the longitude, and h_g is the altitude of the ground station location information. After obtaining the coordinates of the ground and satellite in the ECEF coordinate system, the coordinates for CPF data (x_s, y_s, z_s) and the ground station (x_g, y_g, z_g) are converted once more to the ENU coordinate system for ray-tracing simulation. This conversion must take into account the relative positions of the ground station and the satellite, and the vector (d_x, d_y, d_z) describing this relationship is defined as follows [35]:

$$\begin{aligned} dx &= x_s - x_g \\ dy &= y_s - y_g \\ dz &= z_s - z_g \end{aligned} \tag{7}$$

The satellite position in the ENU coordinate system (e_s, n_s, u_s), relative to the ground station, can be determined using the following conversion matrix:

$$\begin{bmatrix} e_s \\ n_s \\ u_s \end{bmatrix} = \begin{bmatrix} -\sin\lambda_g & \cos\lambda_g & 0 \\ -\sin\phi_g\cos\lambda_g & -\sin\phi_g\sin\lambda_g & \cos\phi_g \\ \cos\phi_g\cos\lambda_g & -\cos\phi_g\sin\lambda_g & \sin\phi_g \end{bmatrix} \begin{bmatrix} dx \\ dy \\ dz \end{bmatrix} \tag{8}$$

The converted trajectory information can be obtained based on the ground stations on Osan and Jeju Island, respectively. Fig. 9(b) illustrates the LEO satellite tracking scenario, where the satellite's trajectory is represented in the ENU coordinate system. In this scenario, the location of the LEO satellite is expressed as range d and altitude h, and the trajectory of this satellite is observed overtime from t_s to t_e.

Fig. 10 shows the detection angle errors when space surveillance radars on the ground station track the actual LEO satellite's trajectories. In this analysis, atmospheric conditions are applied as either normal or duct conditions

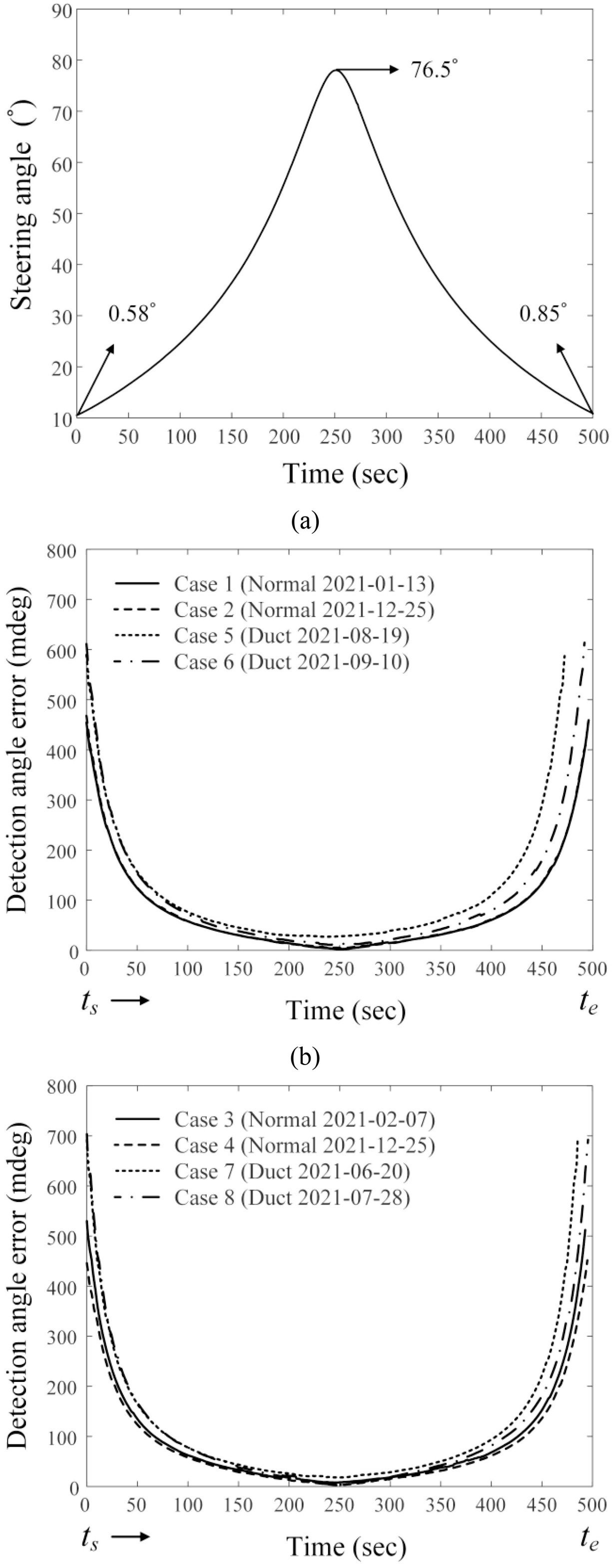

FIGURE 10. Detection angle error during satellite tracking (KOMPSAT-5). (a) an example of a radar's steering angle for the satellite trajectory of Case 1. (b) in the inland (Osan). (c) on the coast (Jeju Island).

as defined in Recommendation ITU-R P.453-13 [28]. The normal condition corresponds to typical atmospheric states in which moderate electromagnetic wave refraction occurs. In

TABLE 3. The detection angle error according to the tracking time in the inland.

Time	Case 1	Case 2	Case 5	Case 6
20 sec.	251 mdeg	246 mdeg	305 mdeg	309 mdeg
250 sec.	5.4 mdeg	2.7 mdeg	28.2 mdeg	12.9 mdeg

TABLE 4. The detection angle error according to the tracking time on the coast.

Time	Case 3	Case 4	Case 7	Case 8
20 sec.	263 mdeg	238 mdeg	331 mdeg	329 mdeg
250 sec.	3.4 mdeg	3.4 mdeg	18.5 mdeg	18 mdeg

contrast, the duct condition indicates that the electromagnetic waves can be strongly refracted toward the Earth's surface. When a satellite is observed, the steering angle of the surveillance radars gradually increases until the satellite passes by the ground station. After this, the steering angle gradually decreases. For example, when surveillance radar tracks the LEO satellite with the trajectory of Case 1, the steering angle varied from 0.58° to 76.37°, as shown in Fig. 10(a). Therefore, the detection angle error is also varied according to the observation time. Fig. 10(b) and (c) represent the detection angle errors in the inland and coast for different dates. Cases 1 to 4 are normal atmospheric conditions, and Cases 5 to 8 are duct conditions with strong atmospheric refractivity. For all the cases, the detection angle errors at specific observation times are listed in Table 3 (inland) and Table 4 (coast). As can be seen in these results, at an observation time of 20 sec., the detection angle error of Case 5 is 305 mdeg, which is greater than that of Case 1 (251 mdeg). In addition, at an observation time of 20 sec., the detection angle error of Case 3 is observed to be 263 mdeg, which is also greater than that of Case 1. This tendency is observed for all the analysis cases. These results mean that the following results: first, detection angle error on the coast is typically greater than that of the inland. Second, strong atmospheric refraction can cause a large detection error. Finally, a great detection angle error may occur when space surveillance radars on the ground station begin tracking the LEO satellite.

IV. CONCLUSION

We investigated the ray-tracing method to estimate the propagation path between a ground station and LEO satellites. To accurately predict a propagation path and detection error, the proposed ray-tracing method adopts the atmospheric refractivity model, which includes the troposphere and the ionosphere. The detection angle errors were examined by changing various conditions such as locations of ground station, satellite trajectories, and observation date. For the inland observatories, the average and deviation of detection error during winter were 43.7 mdeg and 5.9 mdeg, respectively. On the other hand, during summer, an average error of 51.9 mdeg and a deviation of 25.5 mdeg were observed, which were higher than the average detection error during winter. For KOMPSAT-5 satellite trajectories, the maximum detection angle errors observed at the inland and coastal meteorological observatories were 309 mdeg and 331 mdeg, respectively. The results demonstrated that the proposed ray-tracing method is suitable for finding the propagation path between the ground station and the LEO satellites.

REFERENCES

[1] J. Matar, M. Rodriguez-Cassola, G. Krieger, and A. Moreira, "On the equivalence of LEO-SAR constellations and complex high-orbit SAR systems for the monitoring of large-scale processes," *IEEE Geosci. Remote Sens. Lett.*, vol. 21, 2024, Art.no. 8500205.

[2] M. Y. Abdelsadek, G. Karabulut-Kurt, H. Yanikomeroglu, P. Hu, G. Lamontagne, and K. Ahmed, "Broadband connectivity for handheld devices via LEO satellites: is distributed massive MIMO the answer?" *IEEE Open J. Commun. Soc.*, vol. 4, pp. 713–721, 2023.

[3] B. Li, J. Huang, Y. Feng, F. Wang, and J. Sang, "A machine Learning-Based approach for improved orbit predictions of LEO space debris with sparse tracking data from a single station," *IEEE Trans. Aerosp. Electron. Syst.*, vol. 56, no. 6, pp. 4253–4265, Dec. 2020.

[4] N. Khairallah and Z. M. Kassas, "Ephemeris tracking and error propagation analysis of LEO satellites with application to opportunistic navigation," *IEEE Trans. Aerosp. Electron. Syst.*, vol. 60, no. 2, pp. 1242–1252, Apr. 2024.

[5] S. Hamidian and A. R. Kosari, "A PCA-SVM regression model for LEO space debris orbit prediction in an optical Space-Based space surveillance network," *IEEE Access*, vol. 12, pp. 60447–60465, 2024.

[6] M.-H. Golbon-Haghighi, M. Mirmozafari, H. Saeidi-Manesh, and G. Zhang, "Design of a cylindrical crossed dipole phased array antenna for weather surveillance radars," *IEEE Open J. Antennas Propag.*, vol. 2, pp. 402–410, 2021.

[7] S. S. Yoon, J. W. Lee, T.-K. Lee, and J. H. Roh, "Insensitivity characteristics in the dual polarization of deployable CFRP reflector antennas for SAR," *IEEE Trans. Antennas Propag.*, vol. 66, no. 1, pp. 88–95, Jan. 2018.

[8] S. Lee, S. Jo, S. Kim, T.-K. Lee, and J. W. Lee, "Analysis of cross-polarized field by panel misalignment errors in a deployable reflector antenna," *J. Electromagn. Eng. Sci.*, vol. 23, no. 1, pp. 18–26, Jan. 2023.

[9] S. Kim and S. Nam, "Wideband and low-profile array of tightly coupled dipole subarrays," *J. Electromagn. Eng. Sci.*, vol. 24, no. 5, pp. 541–543, Sep. 2024.

[10] X.-W. Guan, L.-X. Guo, Y.-J. Wang, and Q.-L. Li, "Parabolic equation modeling of propagation over terrain using digital elevation model," *Int. J. Antennas Propag.*, vol. 2018, Mar. 2018, Art. no. 1878307.

[11] Q. Guo and Y. Long, "Two-Way parabolic equation method for radio propagation over rough sea surface," *IEEE Trans. Antennas Propag.*, vol. 68, no. 6, pp. 4839–4847, Jun. 2020.

[12] Z. Shuai, G. Li, and L. Wang, "A three-dimensional parabolic equation with fast Reordered-Alternate direction implicit method for radio propagation in inhomogeneous atmospheres," *IET Microw. Antennas Propag.*, vol. 14, no. 1, pp. 86–92, Jan. 2024.

[13] G. Apaydin and L. Sevgi, *Radio Wave Propagation and Parabolic Equation Modeling*, 1st ed. Hoboken, NJ, USA: Wiley, 2017, p. 26.

[14] G. Apaydin, O. Ozgun, M. Kuzuoglu, and L. Sevgi, "A novel two-way finite-element parabolic equation groundwave propagation tool: Tests with canonical structures and calibration," *IEEE Trans. Geosci. Remote Sens.*, vol. 49, no. 8, pp. 2887–2898, Aug. 2011.

[15] M. Fagre, B. S. Zossi, J. Chum, and A. G. Elias, "Simulated high frequency ray paths considering traveling ionospheric disturbances," *SN Appl. Sci.*, vol. 2, p. 615, Mar. 2020.

[16] L. H. Pederick and M. A. Cervera, "Semiempirical model for ionospheric absorption based on the NRLMSISE-00 atmospheric model," *Radio Sci.*, vol. 49, no. 1, pp. 81–93, Feb. 2014.

[17] D. Li, X. Zhu, Z. Dong, A. Yu, and Y. Zhang, "Background tropospheric delay in geosynchronous synthetic aperture radar," *Remote Sens.*, vol. 12, no. 18, p. 3081, Sep. 2020.

[18] Y. Lu, J. Zhang, Y. Guo, L. Wang, and X. Wang, "Real-Time tropospheric delay retrieval from multi-GNSS PPP ambiguity resolution," *Remote Sens.*, vol. 10, no. 12, p. 1964, Dec. 2018.
[19] W. Luo, Z. Liu, and M. Li, "A preliminary evaluation of the performance of multiple ionospheric models in low-and mid-latitude regions of China," *GPS Solut.*, vol. 18, pp. 297–308, Jul. 2014.
[20] J. Liu et al., "Analysis of ionospheric delay correction model performance during geomagnetic storms," *Radio Sci.*, vol. 59, no. 7, 2024, Art. no. e2023RS007803.
[21] K. Liu, Z. Yuan, C. Zhou, Q. Zhu, H. Wang, D. Sheng, and X. Dong, "Integrated High-Accuracy correction technology of Radio-Wave refraction for deep-space (high-orbit) targets," *Atmosphere*, vol. 12, p. 1151, Sep. 2021.
[22] I. P. Shkarofsky, "Generalized Appleton-Hartree equation for any degree of ionization and application to the ionosphere," in *Proc. IRE*, vol. 49, no. 12, pp. 1857–1871, Dec. 1961.
[23] "NeQuick 2 Web model." ICTP. Accessed: Sep. 24, 2024. [Online]. Available: https://t-ict4d.ictp.it/nequick2/nequick-2-web-model
[24] L. Sevgi, *Electromagnetic Modeling and Simulation*. Hoboken, NJ, USA: Wiley-IEEE Press, 2014, p. 324.
[25] Q. Zhang, Y. Tan, G. Ren, and T. Tang, "Ray tracing method of gradient refractive index medium based on refractive index step," *Appl. Sci.*, vol. 11, no. 3, pp. 912–921, Jan. 2021.
[26] A. Lin, "Binary search algorithm," *WikiJ. Sci.*, vol. 2, no. 1, p. 5, 2019, doi: 10.15347/wjs/2019.005.
[27] *Ionospheric Propagation Data and Prediction Methods Required for the Design of Satellite Networks and Systems*, ITU-R Rec. P. 531-14, Int. Telecommun. Union, Geneva, Switzerland, 2019.
[28] *The Radio Refractive Index: Its Formula and Refractivity Data*, ITU-Rec. P. 453-13, Int. Telecommun. Union, Geneva, Switzerland, 2017.
[29] M. Yan, C. Wang, J. Ma, Z. Wang, and B. Yu, "Correction of atmospheric refraction geolocation error for high resolution optical satellite pushbroom images," *Photogramm. Eng. Remote Sens.*, vol. 82, no. 6, pp. 427–435, Jun. 2016.
[30] J. A. Cutler et al., "Radar observations for space domain awareness using leolabs commercial network," *Sensors*, vol. 25, no. 6, p. 2302, Mar. 2024.
[31] L. L. Freitas and E. Costa, "Ray tracing and applications to an evaporation duct model based on data from oceanographic buoy sensors," *J. Microw., Optoelectron. Electromagn. Appl.*, vol. 18, no. 1, pp. 96–113, Mar. 2019.
[32] W. L. Patterson, *User Manual for Advanced Refractive Effects Prediction System (AREPS)*, Space Naval Warfare Syst. Center, San Diego, CA, USA, 2004.
[33] *Effects of Tropospheric Refraction on Radiowave Propagation*, Int. Telecommun. Union, Geneva, Switzerland, ITU-Rec. P. 834-9, 2017.
[34] J. Zhu, "Conversion of earth-centered earth-fixed coordinates to geodetic coordinates," *IEEE Trans. Aerosp. Electron. Syst.*, vol. 30, no. 3, pp. 957–961, Jul. 1994.
[35] D. Kuna, N. Santhosh, and N. K. Perumalla, "Preliminary analysis of standalone Galileo and NavIC in the context of positioning performance for low latitude region," *Procedia Comput. Sci.*, vol. 171, pp. 225–234, Jun. 2020.

JONGHO KEUN received the B.S. degree in information and telecommunication engineering from Dongyang Mirae University, Seoul, Republic of Korea, in 2022. He is currently pursuing the M.S. degree in electronic and electrical engineering from Hongik University, Seoul, in 2024. His research interests include UWB antennas, direction-finding, array antennas, space surveillance system, and propagation environment analysis.

DOYOUNG JANG received the B.S. degree in information and telecommunication engineering from Dongyang Mirae University, Seoul, Republic of Korea, in 2018, and the M.S. and Ph.D. degrees in electronic and electrical engineering from Hongik University, Seoul, in 2020 and 2023, respectively. He was a Research Engineer with MOASOFT, Seoul, from 2015 to 2018, and then from 2024 to 2025, he was a Senior Engineer with Hanwha Systems. He currently joined Dongyang Mirae University as an Assistant Professor. His research interests include array antennas, radars, and electromagnetic wave propagation.

HOSUNG CHOO (Senior Member, IEEE) received the B.S. degree in radio science and engineering from Hanyang University, Seoul, South Korea, in 1998, and the M.S. and Ph.D. degrees in electrical and computer engineering from the University of Texas at Austin, in 2000 and 2003, respectively. In September 2003, he joined the School of Electronic and Electrical Engineering, Hongik University, Seoul, where he is currently a Professor. His principal areas of research include electrically small antennas for wireless communications, reader and tag antenna for RFID, on-glass and conformal antennas for vehicles and aircraft, and array antenna for GPS applications.